# Quasi-one-dimensional antiferromagnetism and multiferroicity in $CuCrO_4$

J. M. Law,[1,2,*] P. Reuvekamp,[1] R. Glaum,[3] C. Lee,[4] J. Kang,[4] M.-H. Whangbo,[4] and R. K. Kremer[1]

[1]*Max-Planck-Institut für Festkörperforschung, Heisenbergstrasse 1, D-70569 Stuttgart, Germany*

[2]*Department of Physics, University of Loughborough, Loughborough, Leicestershire LE11 3TU, England*

[3]*Institut für Anorganische Chemie, Universität Bonn, Gerhard-Domagk-Strasse 1, D-53121 Bonn, Germany*

[4]*Department of Chemistry, North Carolina State University, Raleigh, North Carolina 27695-8204, USA*

(Received 15 April 2011; published 28 July 2011)

The bulk magnetic properties of the new quasi-one-dimensional Heisenberg antiferromagnet, $CuCrO_4$, were characterized by magnetic susceptibility, heat capacity, optical spectroscopy, electron paramagnetic resonance and dielectric capacitance measurements, and density functional evaluations of the intrachain and interchain spin-exchange interactions. We found type-II multiferroicity below the Néel temperature of 8.2(5) K, arising from competing antiferromagnetic nearest-neighbor ($J_{nn}$) and next-nearest-neighbor ($J_{nnn}$) intrachain spin-exchange interactions. Experimental and theoretical results indicate that the ratio $J_{nn}/J_{nnn}$ is close to 2, putting $CuCrO_4$ in the vicinity of the Majumdar-Ghosh point.

DOI: 10.1103/PhysRevB.84.014426 PACS number(s): 75.30.Et, 75.40.Cx, 75.85.+t

## I. INTRODUCTION

Ferroelectricity driven by magnetic ordering in so-called type-II multiferroics exhibits a high potential for technological applications.[1] Switching ferroelectric polarization by a magnetic field or magnetization by an electric field offers unprecedented applications in modern energy-effective electronic data storage technology.[2,3] However, the link of magnetic order and ferroelectricity in type-II multiferroics still remains an intriguing question.[4–6] To elucidate this issue, much attention has been focused lately on the magnetic and magnetoelectric (ME) properties of quasi-one-dimensional (1D) antiferromagnetic (AFM) quantum chain systems, which exhibit incommensurate cycloidal magnetic ordering.[7] Such systems lose inversion symmetry and appear to be suitable candidates for multiferroicity. Incommensurate spin-spiral magnetic ordering occurs in magnetic systems consisting of 1D chains when the intrachain nearest-neighbor (nn) and next-nearest-neighbor (nnn) spin-exchange interactions ($J_{nn}$ and $J_{nnn}$, respectively) are spin-frustrated, as found for compounds with $CuX_2$ ribbon chains made up of $CuX_4$ plaquettes, where $X$ is a suitable anion, e.g., oxygen or a halide. Current examples include $LiCuVO_4$, $NaCu_2O_2$, and $CuCl_2$.[8–14] It is typical that the Cu-$X$-Cu superexchange $J_{nn}$ is ferromagnetic (FM); the Cu-$X\cdots X$-Cu super-superexchange $J_{nnn}$ is AFM and larger in magnitude.[12,15] A cycloidal spin-spiral along a 1D chain induces a macroscopic electric polarization, $\vec{P} \propto \vec{e}_{ij} \times (\vec{S}_i \times \vec{S}_j)$, where $e_{ij}$ is the vector linking the moments residing on adjacent spins $\vec{S}_i$ and $\vec{S}_j$.[16–18]

In an ongoing effort to identify new quantum spin-chain systems that may exhibit spiral magnetic order and ferroelectric polarization, we recently focused our attention on compounds crystallizing with ribbon chains, mainly those belonging to the $CrVO_4$ structure type. The aforementioned structure type features $MO_2$ ribbon chains, where $M$ is a magnetic $3d$ transition metal. Such compounds were recently shown to exhibit exotic magnetic ground states.[19–22] Here, we report on the magnetic and ME properties of another member of this structure type, $CuCrO_4$. Our density functional calculations indicate $J_{nn}$ to be about twice as strong as $J_{nnn}$, putting $CuCrO_4$ in the vicinity of the Majumdar-Ghosh point for which the ground state can be solved exactly.[23] This feature makes $CuCrO_4$ uniquely exceptional since all of the $CuX_2$ ribbon chain systems investigated so far exhibit FM $J_{nn}$ and AFM $J_{nnn}$ spin exchange, where $J_{nnn}$ is considerably larger in magnitude than $J_{nn}$.[9,12,15,24] We demonstrate that $CuCrO_4$ exhibits long-range AFM ordering below ~8.2 K, which is accompanied by a ME anomaly due to possible spin-spiral ordering in the $CuO_2$ ribbon chains.

### A. Crystal structure

$CuCrO_4$ crystallizes in the $CrVO_4$ structure type[25,26] (SG: *Cmcm*, No. 63) with $Cu^{2+}$ ($d^9$, $S = 1/2$) and $Cr^{6+}$ ($d^0$) ions. In the crystal structure of $CuCrO_4$, the axially elongated $CuO_6$ octahedra share edges to form chains running along the $c$ axis [Fig. 1(a)]. These chains are interconnected by $CrO_4$ tetrahedra such that each $CrO_4$ tetrahedron is linked to three $CuO_4$ chains by corner-sharing [Fig. 1(b)]. The $x^2-y^2$ magnetic orbital of each $CuO_6$ octahedron is contained in the $CuO_4$ plaquette with four short Cu-O bonds.[27] Thus, as far as the magnetic properties are concerned, $CuCrO_4$ consists of corrugated $CuO_2$ ribbon chains running along the $c$ axis [Fig. 1(a)]. At room temperature, the Cu$\cdots$Cu distance is 2.945(2) Å and the Cu-O-Cu $\angle$ is 98.1(1)°.

## II. SPIN-EXCHANGE INTERACTIONS

To examine the magnetic properties of $CuCrO_4$, we consider the four spin-exchange paths defined in Fig. 1: the two intrachain exchanges $J_{nn}$ and $J_{nnn}$ as well as the interchain exchanges $J_1$ and $J_2$. To determine the values of $J_{nn}$, $J_{nnn}$, $J_1$, and $J_2$, we examine the relative energies of the five ordered spin states depicted in Fig. 2 in terms of the Heisenberg spin Hamiltonian,

$$H = -\sum J_{ij}\vec{S}_i\vec{S}_j, \qquad (1)$$

where $J_{ij}$ is the exchange parameter (i.e., $J_{nn}$, $J_{nnn}$, $J_1$, and $J_2$) for the interaction between the spin sites $i$ and $j$. Then, by applying the energy expressions obtained for spin dimers with $N$ unpaired spins per spin site (in the present case, $N = 1$),[28] the total spin exchange energies of the five ordered

 

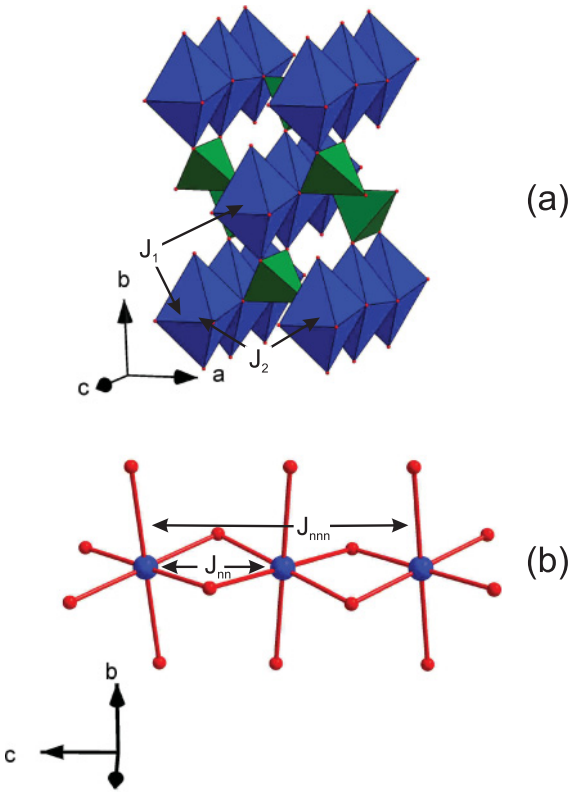


FIG. 1. (Color online) (a) The crystal structure of $CuCrO_4$. The (blue) octahedra are the $CuO_6$ units while the (green) tetrahedra are the $CrO_4$ units. The interchain spin-exchange pathways $J_1$ and $J_2$ are also indicated. (b) A section of the $CuO_2$ ribbon chain highlighting the edge sharing $CuO_4$ plaquettes, with the nn $J_{nn}$ and nnn $J_{nnn}$ spin-exchange pathways labeled.

spin states per four formula units (FU) are given as summarized in Fig. 2. We determine the relative energies of the five ordered spin states of $CuCrO_4$ on the basis of density functional calculations with the Vienna *ab initio* simulation package, employing the projected augmented-wave method,[29–31] the generalized-gradient approximation (GGA) for the exchange and correlation functional,[32] with the plane-wave cutoff energy set to 400 eV, and a set of 64 **k** points for the irreducible Brillouin zone. To account for the strong electron correlation associated with the Cu 3*d* state, we performed GGA plus on-site repulsion (GGA+$U$) calculations with $U_{eff} = 4$ and 6 eV for Cu.[33] The relative energies of the five ordered spin states obtained from our GGA+$U$ calculations are summarized in Fig. 2. Then, by mapping these relative energies onto the corresponding relative energies from the total spin-exchange energies,[27,34–37] we obtain the values of the spin-exchange parameters, $J_{nn}$, $J_{nnn}$, $J_1$, and $J_2$, as summarized in Table I.

The intrachain spin exchanges $J_{nn}$ and $J_{nnn}$ are both AFM and constitute the two dominant spin exchanges in $CuCrO_4$. The interchain parameter $J_2$, connecting Cu atoms related by a translation along $a$, is FM and, depending on the on-site repulsion parameter $U_{eff}$, its magnitude amounts to 15%–20% of the intrachain spin exchange $J_{nn}$. $J_1$, which couples adjacent spin moments that are related by a translation along [110], is AFM and comparatively small. Therefore, to a first

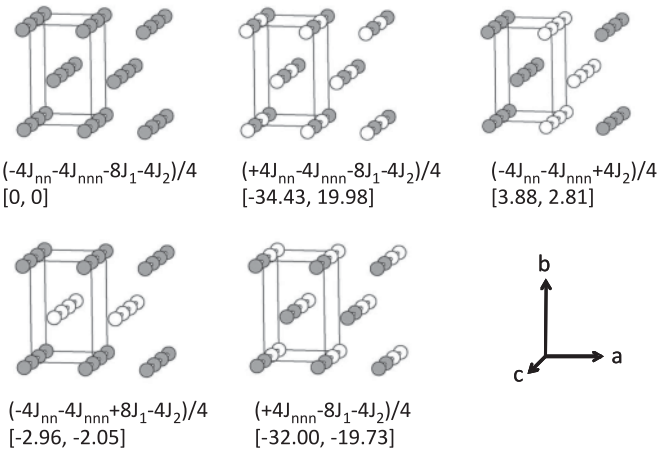


FIG. 2. Five ordered spin states used to extract the values of $J_{nn}$, $J_{nnn}$, $J_1$, and $J_2$, where the $Cu^{2+}$ sites with different spins are denoted by filled and empty circles. For each ordered spin state, the expression for the total spin-exchange energy per four FU's is given, and the two numbers in square brackets (from left to right) are the relative energies in meV per four FU's, obtained from the GGA+$U$ calculations with $U_{eff} = 4$ and 6 eV, respectively.

approximation, $CuCrO_4$ can be described as a quasi-1D Heisenberg magnet with nn and nnn spin-exchange interactions, both being AFM. Since these 1D chains are connected by weak interchain exchanges ($J_1$ and $J_2$), long-range ordering will eventually take place at low temperatures.

## III. EXPERIMENTAL

A polycrystalline sample of $CuCrO_4$ was prepared by separately dissolving equimolar amounts of anhydrous copper(II)acetate and chromium(VI)oxide in distilled water, similar to the recipe given by Arsene *et al.*[38] The two solutions were mixed and boiled to dryness. The resulting powder was heat-treated in air at a temperature of 150 °C for 2 days. The phase purity of the sample was checked by x-ray powder diffraction measurements using a STOE STADI-P diffractometer with monochromated Mo $K\alpha_1$ radiation. The

TABLE I. Spin-exchange parameters $J_{nn}$, $J_{nnn}$, $J_1$, and $J_2$ (in K) of $CuCrO_4$ obtained from GGA+$U$ calculations with $U_{eff} = 4$ and 6 eV. The left column for each $U_{eff}$ contains the theoretical results, while the values in the right column are the scaled theoretical results such that $J_{nnn}$ equals the experimental finding, −27 K. The rightmost column summarizes the experimentally found spin-exchange values. The final row show the Curie-Weiss temperatures of the scaled GGA+$U$ spin-exchange parameters, calculated using the mean-field expression $\theta_{CW} = \frac{1}{3}\sum_i z_i J_i S(S+1)$, where $z_i$ is the number of neighbors with which a single atom interacts with the spin exchange $J_i$ and the experimentally observed values (see below).

| $J_i$ | $U_{eff} = 4$ eV | | $U_{eff} = 6$ eV | | Experiment |
|---|---|---|---|---|---|
| $J_{nn}$ | −199.7(1.0) | −63.8 | −115.9(1.0) | −55.4 | −54 |
| $J_{nnn}$ | −85.8(0.43) | −27 | −56.5(0.49) | −27 | −27 |
| $J_1$ | −8.6(0.04) | −2.7 | −6.00(0.05) | −2.9 | |
| $J_2$ | +31.1(0.16) | +9.8 | +22.3(0.19) | +10.7 | +12 |
| $\theta_{CW}$ | | −43.2 | | −38.8 | −56/−60 |

powder pattern was analyzed using the Rietveld profile refinement method employed within the Fullprof Suite.[39] No other reflections besides those of $CuCrO_4$ were observed.

Powder reflectance spectra of $CuCrO_4$ were collected at room temperature using a modified CARY 17 spectrophotometer, equipped with an integrating sphere. The spectrometer was operated in the single-beam mode using $BaSO_4$ as a reflectance (white) standard. $CuCrO_4$ powder was mixed with $BaSO_4$ in a volumetric ratio $CuCrO_4$:$BaSO_4$ ~1:5.

Temperature-dependent electron paramagnetic resonance (EPR) spectra of an ~5 mg polycrystalline sample, contained within an EPR low-background suprasil© quartz tube, were collected using ~9.5 GHz microwave radiation [Bruker ER040XK microwave X-band spectrometer, Bruker BE25 magnet equipped with a BH15 field controller calibrated against Diphenylpicrylhydrazyl (DPPH)].

The molar magnetic susceptibilities, $\chi_{mol}$, of a polycrystalline sample weighting ~84 mg were measured with various fields between 2 and 350 K using a SQUID magnetometer (MPMS, Quantum Design). The raw magnetization data were corrected for the magnetization of the sample container.

The specific heats, $C_p$, of a powder sample weighting ~2.4 mg were determined as a function of the temperature and magnetic field with a relaxation-type calorimeter (PPMS, Quantum Design) for the temperature range 0.4–50 K and magnetic fields up to 9 T.

The relative dielectric constant, $\epsilon_r$, was measured at a constant frequency and excitation voltage, 1000 Hz and 15 V, respectively, with an Andeen-Hagerling 2700A capacitance bridge on a compacted powder (thickness: ~0.8 mm, ∅: 3.6 mm).

## IV. RESULTS AND DISCUSSION

Figure 3 shows the measured and simulated x-ray powder diffraction patterns of the sample of $CuCrO_4$ used for all subsequent characterization. The refined atomic parameters and the lattice parameters are summarized in Table II and were found to be in good agreement with the previously published single-crystal results.[26]

TABLE II. Atomic positional parameters of $CuCrO_4$ (SG: *Cmcm*) as obtained from a profile refinement of the x-ray powder diffraction pattern, collected at room temperature. The lattice parameters amount to $a = 5.4388(5)$ Å, $b = 8.9723(8)$ Å, and $c = 5.8904(6)$ Å.

| Atom | Wyckoff site | $x$ | $y$ | $z$ | $B_{iso}$ (Å$^2$) |
|---|---|---|---|---|---|
| Cu | 4a | 0 | 0 | 0 | 0.09(8) |
| Cr | 4c | 0 | 0.3700(3) | 0.25 | 0.90(8) |
| O1 | 8f | 0 | 0.2652(5) | 0.0320(9) | 0.80(12) |
| O2 | 8g | 0.2326(7) | −0.0198(6) | 0.25 | 0.80(12) |

Figure 4 displays the optical spectrum of $CuCrO_4$, which is consistent with the deep brownish-red color of the $CuCrO_4$ powder. The spectrum is dominated by a strong absorption band centered at 21 500 cm$^{-1}$ (466 nm), which we attribute to an $O^{2-} \rightarrow Cr^{6+}$ charge-transfer transition, in agreement with observations for other hexavalent chromates.[40,41] In the near-infrared regime (NIR), the spectrum exhibits a maximum at $\tilde{\nu}_3 = 13\,000$ cm$^{-1}$ with a tail extending down to ~7000 cm$^{-1}$. Two subsequent faint shoulders are seen within the slope at $\tilde{\nu}_2 = 11\,000$ cm$^{-1}$ and $\tilde{\nu}_1 \sim 8000$ cm$^{-1}$.

Using ligand-field considerations (see below), the observed absorption bands ($\tilde{\nu}_1$, $\tilde{\nu}_2$, and $\tilde{\nu}_3$) can be assigned to $Cu^{2+}$ *d-d* transitions, $^2B_{1g} \rightarrow {}^2A_{1g}$ ($z^2 \rightarrow x^2 - y^2$), $^2B_{1g} \rightarrow {}^2B_{2g}$ ($xy \rightarrow x^2 - y^2$), and $^2B_{1g} \rightarrow {}^2E_g$ ($xz, yz \rightarrow x^2 - y^2$), respectively.[43–46]

From $\tilde{\nu}_1$, $\tilde{\nu}_2$, and $\tilde{\nu}_3$, the crystal-field splitting, $10Dq$ for $CuO_6$, can be calculated using the relation

$$10Dq = \tilde{\nu}_3 - \left(\frac{\tilde{\nu}_3 - \tilde{\nu}_2}{3}\right) - \left(\frac{\tilde{\nu}_1}{2}\right),$$

which yields a value of $10Dq$ ~8300 cm$^{-1}$. This value is similar to crystal-field-splitting values previously reported, e.g., for $Cu^{2+}$ aquo-complexes.[43]

uv/vis spectra for $CuCrO_4$ have been reported before by Baran, and an assignment of the observed transitions has been

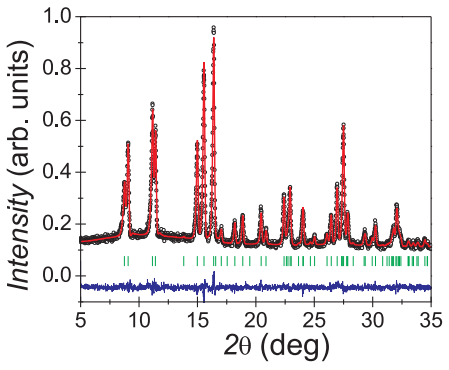


FIG. 3. (Color online) (o): Measured x-ray diffraction pattern of $CuCrO_4$ (wavelength 0.709 Å Mo $K\alpha_1$ radiation). Solid (red) line: Fitted pattern ($R_p = 3.42\%$, reduced $\chi^2 = 1.15$) using the parameters given in Table II. Solid (blue) line (offset): Difference between measured and calculated patterns. The positions of the Bragg reflections used to calculate the pattern are marked by the (green) vertical bars in the lower part of the figure.

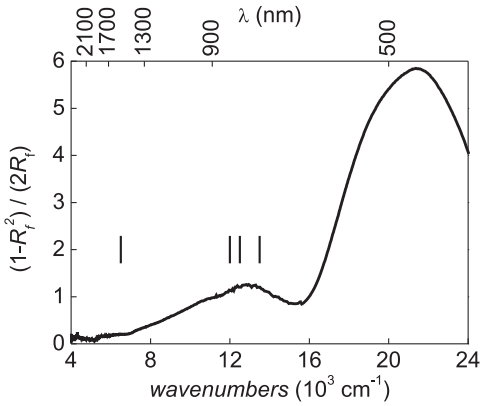


FIG. 4. Powder reflectance spectrum of $CuCrO_4$. Black vertical bars mark the ligand-field transition energies, for the $CuO_6$ distorted octahedron, obtained from AOM calculations. We show the Kubelka-Munk relation, $(1 - R_f)^2/(2R_f)$, where $R_f = I(CuCrO_4)/I(BaSO_4)$ and $I(CuCrO_4)$ and $I(BaSO_4)$ are the reflected light intensities of the sample and the $BaSO_4$ standard, respectively.[42]

TABLE III. Parameter used in the AOM calculations. The equatorial plane forms a rectangle with the equatorial $O_{eq}$-Cu-$O_{eq}$ bonds enclosing an $\angle$ of 81.92° and 98.08°, respectively. The Racah parameters amounted to $B = 992$ cm$^{-1}$, $C = 3770$ cm$^{-1}$ yielding a ratio $C/B = 3.8$, as given for the free $Cu^{2+}$ ion.[43] As for the aquo-complex, the nephelauxetic ratio $\beta$ was chosen to be 0.80, and the spin-orbit coupling parameter $\zeta = 664$ cm$^{-1}$ was reduced by 20% as compared to the free ion value.[43,53]

| | $O_{eq}$ | $O_{ax}$ |
|---|---|---|
| $d$ (Cu-O) (Å) | 1.965 (4×) | 2.400 (2×) |
| $e_\sigma$ (cm$^{-1}$) | 5600 | 2061 |
| $e_{\pi,x}$ (cm$^{-1}$) | 1400 | 515 |
| $e_{\pi,y}$ (cm$^{-1}$) | 1400 | 515 |

been proposed.[47] Based on calculations within the framework of the angular overlap model (AOM),[43–46] we argue that this assignment has to be revised.

Within the AOM model, the pairwise interactions of the ligands with the $d$ orbitals are encoded into the parameters $e_\sigma$, $e_{\pi,x}$, and $e_{\pi,y}$, which take care of interaction along and perpendicular to the Cu-$O_i$ ($i = 1, \ldots, 6$) bond, respectively. The energies of the individual $d$ orbitals are obtained by summation over all pairwise interactions. The variation of the AOM parameters $e_{\sigma i}$ with the Cu-$O_i$ distance has been taken care of by

$$e_{\sigma i} \propto 1/r_i^n.$$

An exponent of $n \approx 5$ is derived from electrostatic and covalent theoretical bonding considerations.[42,48,49] Measurements of the pressure dependence of $10Dq$ pointed to a similar exponent $5 \leqslant n \leqslant 6$.[50] For the sake of simplicity, we have chosen $e_{\pi,x} = e_{\pi,y} = 1/4e_\sigma$. AOM calculations have been performed using the program CAMMAG.[51,52] Table III summarizes the parameters that have been used for these calculations. The resulting transition energies marked by vertical bars in Fig. 4 are in good agreement with the centers of the experimentally observed absorption features.

In addition to the energy of the excited electronic states of the isolated $CuO_6$ unit, its magnetic properties are also obtained from the AOM calculations. The parametrization leads to an average $g_{av} = 2.18$ and a strongly anisotropic $g$ tensor with $g_x = 2.07$, $g_y = 2.07$, and $g_z = 2.39$ along the principal axes. The $z$ direction of the $g$ tensor lies along the Cu-$O_{ax}$ bond direction.

The results of the specific-heat measurements for magnetic fields of 0 and 9 T are displayed in Fig. 5. The 0 T data reveal a rather broad, smeared, λ-type anomaly centered at 8.2(5) K marking the onset of long-range magnetic ordering. Within experimental error, the data measured in a magnetic field of 9 T are identical to those obtained at 0 T. The plot of $C_p/T$ versus $T$ given in the lower right inset of Fig. 5 enables an estimation of the entropy contained within the anomaly, which equates to ~0.6 J/mol K or ~10% of the expected entropy of an $S = 1/2$ system, $R$ ln(2), where $R$ is the molar gas constant. 90% of the entropy has already been removed by short-range AFM ordering above $T_N$.

At low temperatures, the heat capacity is comprised of a phonon and magnon contribution. The temperature

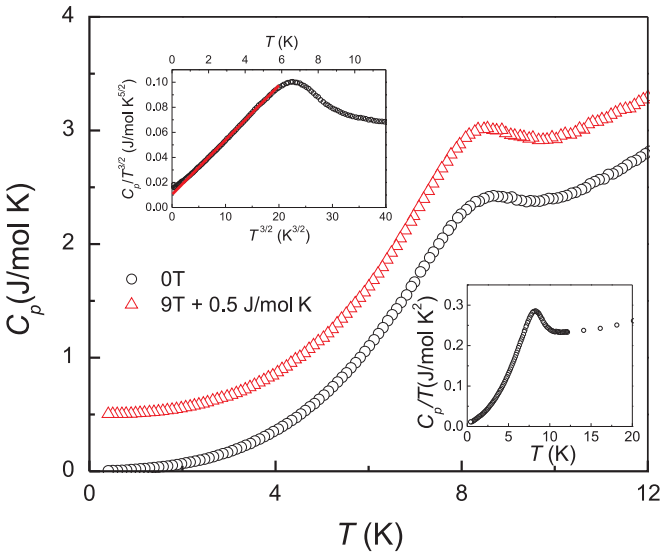


FIG. 5. (Color online) (Black) o and (red) △: Heat capacity of $CuCrO_4$ at 0 and 9 T, respectively. The latter data have been shifted by +0.5 J/mol K. Upper left inset: $C_p/T^{3/2}$ plotted vs $T^{3/2}$ to highlight the low-temperature $T^{3/2}$ power law. The (red) solid line is a fit of the data to Eq. (2) with parameters given in the text. Lower right inset: $C_p/T$ depicted against $T$ in the low-temperature regime.

dependence of the phonon contributions to the heat capacity can be described by a Debye-$T^3$ power law. The magnon heat capacity at low temperatures varies with a power law depending on the spin-wave dispersion relation and the dimensionality of the lattice. For a three-dimensional (3D) magnetic lattice, one obtains a $T^3$ power law for AFM magnons and a $T^{3/2}$ power law for FM magnons.[54] The $C_p/T^{3/2}$ versus $T^{3/2}$ plot shown in the upper left inset of Fig. 5 demonstrates that at low temperatures, the heat capacity conforms well to a $T^{3/2}$ power law, with the coefficient of the FM magnon contribution given by the nonzero intercept with the ordinate, $\gamma$, according to

$$C_p/T^{3/2} = \beta T^{3/2} + \gamma, \tag{2}$$

where $\beta$ is related to the Debye temperature $\theta_D(0)$ at zero temperature via

$$\beta = M R \frac{12\pi^4}{5} \left(\frac{1}{\theta_D}\right)^3, \tag{3}$$

with $M = 6$ being the number of atoms per formula unit of $CuCrO_4$. By using Eq. (3), we ascertain $\theta_D(T \to 0)$ to be

$$\theta(T \to 0) = 138(3) \text{ K},$$

and from the intercept and Eq. (2) we obtain $\gamma$ as

$$\gamma = 1.03(2) \times 10^{-2} \text{ J/mol K}^{5/2}.$$

Figure 6 summarizes the results of our EPR measurements. Near 3.4 kOe, a single rather broad (peak-to-peak linewidth $\Delta H_{pp} \approx 0.8$–1 kOe) symmetric resonance line was observed. It can be well fitted to the derivative of a single Lorentzian

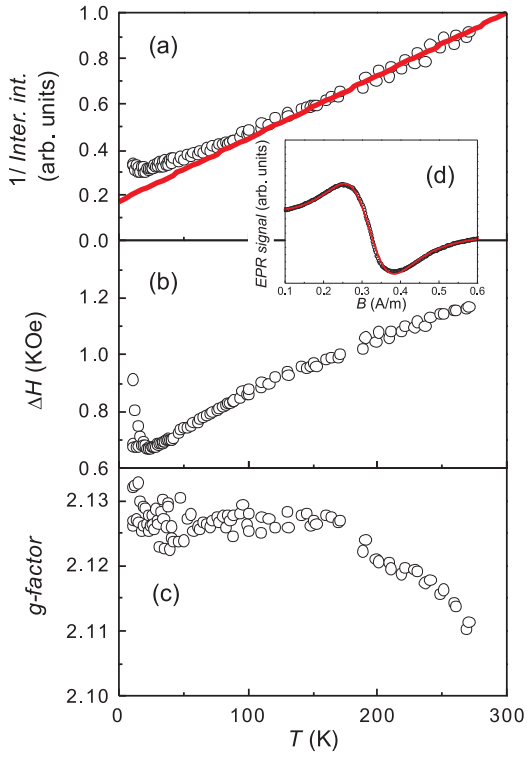


FIG. 6. (Color online) Results of the EPR measurements on a polycrystalline sample of $CuCrO_4$. (a) (o) Inverse of the integrated intensity. The (red) solid line is a fit of Eq. (5) to the high-temperature data ($T \geqslant 150$ K). (b) (o) The fitted half-width at half-maximum (HWHM) vs temperature. (c) (o) $g$ factor vs temperature. (d) (o) EPR spectrum of $CuCrO_4$ measured at RT with ∼9.45 GHz vs applied magnetic field. The (red) solid line represents the fitted derivative of a Lorentzian absorption line Eq. (4) to the measured spectrum.

absorption line with a small contribution $|\alpha| \leqslant 0.04$ of dispersion according to

$$\frac{dP_{\rm abs}}{dH} \propto \frac{d}{dH}\frac{\Delta H + \alpha(H - H_{\rm res})}{(H - H_{\rm res})^2 + \Delta H^2} + \frac{\Delta H + \alpha(H + H_{\rm res})}{(H + H_{\rm res})^2 + \Delta H^2}. \tag{4}$$

As the linewidth [half-width at half-maximum (HWHM)], $\Delta H$, is of the same order of magnitude as the resonance field, $H_{\rm res}$ [see Fig. 6(a)], in Eq. (4) we took into account both circular components of the exciting linearly polarized microwave field and therefore also included the resonance at negative magnetic fields centered at $-H_{\rm res}$.

The resonance field of the room-temperature powder spectrum corresponds to a $g$ factor of 2.117(2). Upon cooling, a slight increase of the $g$ factor with saturation to a value of ∼2.125 below 150 K was observed [Fig. 6(c)]. Such a value is somewhat lower than the expected average value $g_{\rm av}$ ascertained from the AOM calculations. The resonance line is too broad to resolve the anisotropic $g$ factors, which range between ∼2.39 and ∼2.07 (see above).

The integrated intensity of the EPR resonance, $I(T)$, which is proportional to the spin susceptibility, increases with decreasing temperature down to ∼15 K, where a hump occurs. Above ∼150 K, $I(T)$ follows a Curie-Weiss-type temperature dependence,

$$I(T) \propto \frac{1}{T - \theta_{\rm EPR}}, \tag{5}$$

with

$$\theta_{\rm EPR} \approx -60(5)\ {\rm K}.$$

The negative $T$-axis intercept indicates predominant AFM spin-exchange interactions. Deviations from the Curie-Weiss-type temperature dependence are ascribed to short-range AFM correlations, which start to develop below ∼150 K, similar to the behavior of the dc magnetic susceptibility (see below). The decrease of the integrated intensity below ∼15 K signals the onset of long-range ordering.[55]

The magnitude and temperature dependence of the EPR linewidth, $\Delta H$, are similar to those observed for the inorganic spin-Peierls system $CuGeO_3$ or the frustrated AFM 1D system $LiCuVO_4$.[56,57] The linewidth exhibits a concave temperature dependence with a linear increase at low temperatures, and for $T \to \infty$ one extrapolates a saturation value of ∼1.4 kOe.

If we assume that the temperature-dependent broadening of the EPR resonance line is due to anisotropic or antisymmetric components in the exchange Hamiltonian, the constant high-temperature value can be estimated from the Kubo-Tomita limit as[58]

$$\Delta H(T \to \infty) \approx \frac{1}{g\mu_B}\frac{\delta^2}{J}, \tag{6}$$

where $\delta$ indicates the deviations from the symmetric Heisenberg spin exchange and $J$ is the AFM symmetric intrachain exchange. If for $CuCrO_4$ we associate $J$ with the nn spin exchange, ∼60 K (see below), we can estimate a $\delta$ of ∼3 K, i.e., 5% of the symmetric exchange.

The linear slope of the linewidth at low temperatures can be explained using the formalism put forth by Oshikawa and Affleck[59,60] predicting

$$\Delta H(T) \propto \frac{\delta^2}{J^2}T. \tag{7}$$

We find a linear slope, indicative of a 1D AFM system, of ∼2.5 Oe/K, similar to that observed for $CuGeO_3$ (∼4.5 Oe/K).[56]

The magnetic susceptibility of a polycrystalline sample of $CuCrO_4$ was measured in magnetic fields of 1, 3, 5, and 7 T. Above ∼20 K, the susceptibilities are independent of the magnetic field, indicating negligible ferromagnetic impurities. The susceptibilities, $\chi_{\rm mol}(T)$, above ∼150 K follow the modified Curie-Weiss law,

$$\chi_{\rm mol}(T) = \frac{C}{T - \Theta} + \chi_{\rm dia} + \chi_{\rm VV}. \tag{8}$$

$C$ is the Curie constant pertaining to the spin susceptibility of the $Cu^{2+}$ entities, $C = N_A g^2 \mu_B^2 S(S+1)/3k_B$. $\chi_{\rm dia}$ refers to the diamagnetic susceptibilities of the electrons in the closed shells, which can be estimated from the increments given by Selwood, which equate to $-62 \times 10^{-6}$ cm$^3$/mol.[61]

At high temperatures, $T \geqslant 150$ K, we fitted the molar susceptibility to the aforementioned modified Curie-Weiss

law Eq. (8). We found the best agreement with the following parameters:

$$g = 2.17(2) \quad \text{and} \quad \theta = -56(1)\ \text{K}$$

and

$$\chi_{\text{dia}} + \chi_{\text{VV}} \approx +20 \times 10^{-6}\ \text{cm}^3/\text{mol}.$$

This puts the Van Vleck contribution to $\approx +80 \times 10^{-6}$ cm$^3$/mol, which is in reasonable agreement with what has been found for other $Cu^{2+}$ compounds (see Ref. 12 and references therein). The fitted $g$ factor is in good agreement with optical spectroscopy and the Curie-Weiss temperature is negative and in accordance with $\theta_{\text{EPR}}$.

Below 150 K, there are deviations from the Curie-Weiss law attributed to increasing AFM short-range correlations. The susceptibility passes through a broad shoulder with a subsequent kink at ~8 K, whereupon it becomes field-dependent, with a tendency to diverge for small fields. With increasing fields, the divergence is suppressed and the kink becomes more apparent. By 7 T, a pronounced rounded hump with a maximum at 14.2(2) K and a subsequent dip at 8.0(5) K becomes clearly visible.

In general, GGA+$U$ calculations overestimate the spin-exchange constants typically by a factor up to 4, in our case 2.[34,35,62] By taking this into account and by using a mean-field approach, one calculates, from the spin-exchange parameters summarized in Table II, a (negative) Curie-Weiss temperature ranging between −38 and −45 K, consistent with the experimental observations.

Our GGA+$U$ calculations indicate that $CuCrO_4$ can be described by a Heisenberg 1D chain with AFM nn and AFM nnn spin exchanges, with significantly weak interchain interactions ($J_2/J_{\text{nn}} < 0.19$). Therefore, we modeled the magnetic susceptibility of $CuCrO_4$ against exact diagonalization results for the susceptibility $\chi_{\text{chain}}(g,\alpha,J_{\text{nnn}})$ of a single chain provided by Heidrich-Meissner *et al.*,[63,64] with

$$\alpha = J_{\text{nn}}/J_{\text{nnn}}. \tag{9}$$

Interchain spin exchange is treated within a mean-field approach according to[65]

$$\chi_{\text{mol}}(T) = \frac{\chi_{\text{chain}}(T)}{1 - \lambda\,\chi_{\text{chain}}(T)} + \chi_0. \tag{10}$$

By using the already known values, $\chi_0 = \chi_{\text{dia}} + \chi_{\text{VV}} = +20 \times 10^{-6}$ cm$^3$/mol as found from the fit of the high-temperature magnetic susceptibility and a $g$ factor of 2.13 obtained from the EPR measurements, the simulated results can be compared to experimental data. The mean-field parameter, λ, in Eq. (10) can be ascribed to the interchain spin-exchange interactions according to[65]

$$\lambda = (z_1\,J_1 + z_2\,J_2)/N_A g^2 \mu_B^2, \tag{11}$$

wherein $z_1 = 4$ and $z_2 = 2$ count the number of spin moments with which a chain/spin interacts through the interchain spin-exchange interactions, $J_1$ and $J_2$, respectively. Guided by the GGA+$U$ results, the ratio $\alpha$ is positive and in the regime of 1.5–2.5. Within this range for $\alpha$, we find the best agreement of our experimental data with the model calculations for

$$\alpha \approx 2, \quad \text{implying} \quad J_{\text{nnn}} = -27(2)\ \text{K},$$

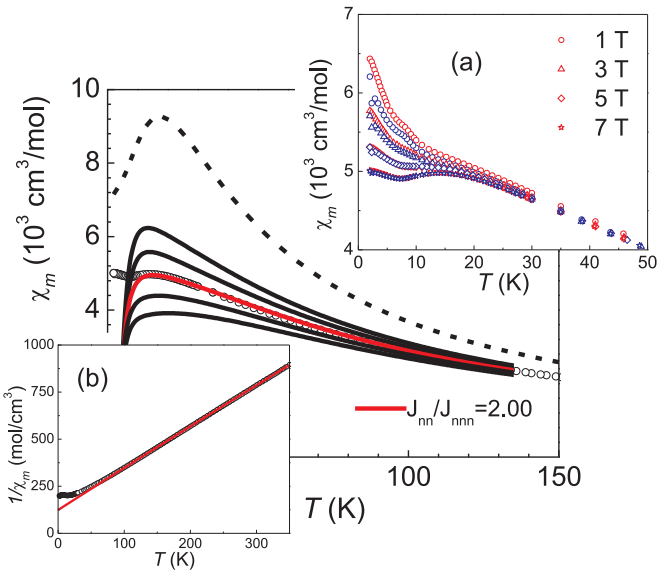


FIG. 7. (Color online) (main panel) (o) Temperature dependence of the molar magnetic susceptibility, $\chi_m$, taken at 7 T. Colored solid lines represent the exact diagonalization results by Heidrich-Meissner *et al.* for various ratios of $J_{\text{nn}}/J_{\text{nnn}}$: 1.5, 1.75, 2 (red solid line), 2.25, and 2.5, from top to bottom, respectively. See text for more details. The dashed line is the magnetic susceptibility of an $S = 1/2$ Heisenberg chain with afm uniform nn spin exchange of −27 K.[66] (a) Red symbols: heating data, blue symbols: cooling data. $\chi_{\text{mol}}$ vs temperature for various magnetic field. (b) (o) Reciprocal molar susceptibility vs temperature with a fit [(red) solid line] to a modified Curie-Weiss law Eq. (8).

and a positive λ, which amounts to

$$\lambda = 7(1)\ \text{mol/cm}^3.$$

Figure 7 shows a comparison of the measured data and the mean-field corrected exact diagonalization results.

$\lambda > 0$ indicates that the dominant interchain spin exchange is FM, consistent with our density functional calculations. The DFT calculations indicate $J_1 \approx -1/4 \times J_2$, irrespective of $U_{\text{eff}}$. From Eq. (11) using $\lambda = 7(1)$ mol/cm$^3$, we derive a value for $J_2$ that amounts to

$$J_2 = 12(2)\ \text{K}.$$

This value is in good agreement with the scaled DFT result; see Table I.

The interchain spin exchange can also be estimated from the Néel temperature, $T_N$, which, according to the heat-capacity data, amounts to (see above)

$$T_N \approx 8.2(5)\ \text{K}.$$

Yasuda *et al.* calculated the Néel temperature of a quasi-1D Heisenberg antiferromagnet on a cubic lattice with the isotropic interchain coupling $J_\perp$, inducing 3D long-range magnetic ordering at a Néel temperature, $T_N$,[67]

$$T_N/|J_\perp| = 0.932\sqrt{\ln(A) + \tfrac{1}{2}\ln[\ln(A)]}, \tag{12}$$

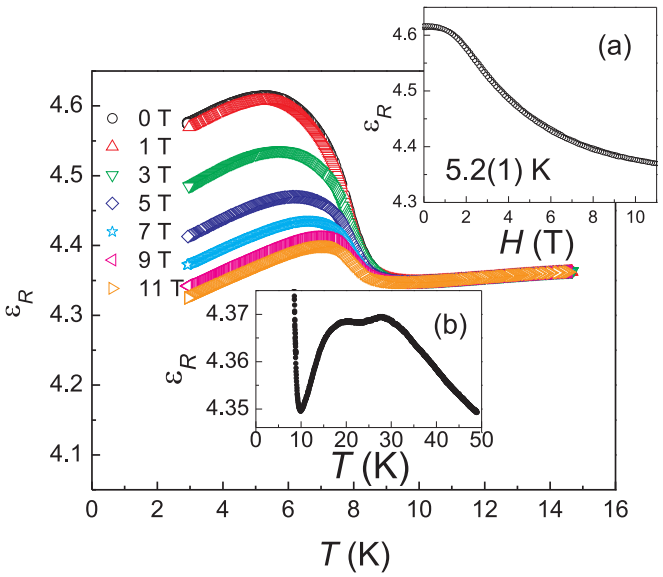


FIG. 8. (Color online) (a) Colored symbols represent the relative dielectric constants, $\epsilon_r$, vs temperature for different applied magnetic fields, as given in the legend. (b) The zero-field relative dielectric constant is shown by the solid black line within a greater temperature range. (c) (o) The relative dielectric constant vs applied magnetic field at a temperature of 5.2(1) K.

where $A = 2.6J_{\parallel}/T_N$ and $J_{\parallel}$ is the intrachain spin-exchange constant. If we assume $J_{\parallel}$ to be our $J_{\rm nn} \sim -60$ K, we find the interchain coupling to be

$$|J_{\perp}| \approx 5 \text{ K},$$

consistent with the value obtained from $\lambda$. The differences may arise, since our real system has two different interchain coupling constants, $J_1$ and $J_2$, as indicated by our density functional calculations. Additionally, $CuCrO_4$ has a nnn spin exchange $J_{\rm nnn}$, which is not included in Yasuda's model.

Figure 8 displays the temperature and magnetic-field dependence of the relative dielectric constant, $\epsilon_r$, of a compacted polycrystalline sample of $CuCrO_4$.

At room temperature, a value of $\sim$48 was found for $\epsilon_r$. With decreasing temperature, $\epsilon_r$ is seen to decrease in a smooth fashion, until it passes through a shallow double maximum between 35 and 15 K, possibly indicating some magnetostriction induced by short-range magnetic ordering processes above $T_N$ [see Fig. 8, inset (b)]. At 10 K, a value of $\epsilon \sim 4.35$ was measured. Long-range magnetic ordering leads to a sizable ME effect as evidenced in the $\epsilon_r$, but with a rather broad anomaly extending over the whole temperature range down to 3 K. Indication of a sharp spike near $T_N$, as is frequently found in multiferroic systems, has not been seen. Similar broad anomalies, originating at $T_N$, have been in seen in $CuCl_2$ and $CuBr_2$.[68,69] In zero field, a steep increase of $\epsilon_r$ is seen to occur below $\sim$8.5 K with a broad slightly asymmetric hump centered at $\sim$5.35 K. In zero field, the increase of $\epsilon_r$ from the paramagnetic phase to the maximum of the hump amounts to $\sim$6%. Applying a magnetic field decreases the ME anomaly and moves the maximum to higher temperatures. The onset of the ME anomaly is not seen to move, in accordance with the aforementioned $C_p$ measurements [see Fig. 8, inset (c)]. The decrease of $\epsilon_r$ with a magnetic field starts above $\sim$1 T and tends to saturation at sufficiently high fields.

## V. CONCLUSION

In summary, $CuCrO_4$ represents a new 1D quantum antiferromagnet with a remarkable pronounced ME anomaly below the Néel temperature of 8.2 K. Our density functional calculations indicate that, to a first approximation, the spin lattice of $CuCrO_4$ is a 1D Heisenberg chain with the unique situation that both nn and nnn spin exchanges are AFM. $J_{\rm nn}/J_{\rm nnn}$ is found to be close to 2, which places $CuCrO_4$ in the vicinity of the Majumdar-Ghosh point. There one could expect an incommensurate magnetic structure along the $c$ axis, with the $c$-axis magnetic unit cell being approximately $3/2 \times c$. The presence of sizable ferromagnetic interchain spin-exchange interaction leads to long-range ferromagnetic ordering between individually antiferromagnetically ordered chains. The occurrence of the rather large ME anomaly below the Néel temperature is taken as evidence for noncollinear, possibly helicoidal, spin ordering in the 1D chains. $CuCrO_4$, therefore, represents a new interesting example for an unusual type-II multiferroicity system. Neutron scattering investigations are scheduled to clarify the exact nature of the magnetic ground state of $CuCrO_4$.

## ACKNOWLEDGMENTS

The authors would like to thank S. Höhn, E. Brücher, and G. Siegle for experimental assistance, and T. Dahmen for the sample preparation. Work at NCSU was supported by the Office of Basic Energy Sciences, Division of Materials Sciences, US Department of Energy, under Grant No. DE-FG02-86ER45259, and also by the computing resources of the NERSC center and the HPC center of NCSU.

*j.law@fkf.mpg.de

[1]For a classification of the types of multiferroicity, see, e.g., D. Khomskii, Physics **2**, 20 (2009).
[2]O. Auciello, J. F. Scott, and R. Ramesh, Phys. Today **51**, 22 (1998).
[3]N. A. Spaldin, S.-W. Cheong, and R. Ramesh, Phys. Today **63**, 38 (2010).
[4]M. Mostovoy, Phys. Rev. Lett. **96**, 067601 (2006).
[5]S.-W. Cheong and M. Mostovoy, Nat. Mater. **6**, 13 (2007).
[6]Y. Tokura and S. Seki, Adv. Mater. **22**, 1554 (2010).
[7]J. van den Brink and D. I. Khomskii, J. Phys. Condens. Matter **20**, 434217 (2008).
[8]B. J. Gibson, R. K. Kremer, A. V. Prokofiev, W. Assmus, and G. J. McIntyre, Physica B **350**, e253 (2004).
[9]M. Enderle, C. Mukherjee, B. Fåk, R. K. Kremer, J.-M. Broto, H. Rosner, S.-L. Drechsler, J. Richter, J. Malek, A. Prokofiev, W. Assmus, S. Pujol, J.-L. Raggazzoni, H. Rakoto,

M. Rheinstädter, and H. M. Rønnow, Europhys. Lett. **70**, 237 (2005).
[10]L. Capogna, M. Mayr, P. Horsch, M. Raichle, R. K. Kremer, M. Sofin, A. Maljuk, M. Jansen, and B. Keimer, Phys. Rev. B **71**, 140402(R) (2005).
[11]T. Kimura, Y. Sekio, H. Nakamura, T. Siegrist, and A. P. Ramirez, Nat. Mater. **7**, 291 (2008).
[12]M. G. Banks, R. K. Kremer, C. Hoch, A. Simon, B. Ouladdiaf, J.-M. Broto, H. Rakoto, C. Lee, and M.-H. Whangbo, Phys. Rev. B **80**, 024404 (2009).
[13]L. Capogna, M. Reehuis, A. Maljuk, R. K. Kremer, B. Ouladdiaf, M. Jansen, and B. Keimer, Phys. Rev. B **82**, 014407 (2010).
[14]M. Mourigal, M. Enderle, R. K. Kremer, J. M. Law, and B. Fåk, Phys. Rev. B **83**, 100409(R) (2011).
[15]H.-J. Koo, C. Lee, M.-H. Whangbo, G. J. McIntyre, and R. K. Kremer, Inorganic Chemistry **50**, 3582 (2011).
[16]H. Katsura, N. Nagaosa, and A. V. Balatsky, Phys. Rev. Lett. **95**, 057205 (2005).
[17]I. A. Sergienko and E. Dagotto, Phys. Rev. B **73**, 094434 (2006).
[18]H. J. Xiang and M.-H. Whangbo, Phys. Rev. Lett. **99**, 257203 (2007).
[19]J. P. Attfield, P. D. Battle, and A. K. Cheetham, J. Solid State Chem. **57**, 357 (1985).
[20]R. Glaum, M. Reehuis, N. Stüßer, U. Kaiser, and F. Reinauer, J. Solid State Chem. **126**, 15 (1996).
[21]J. M. Law, C. Hoch, M.-H. Whangbo, and R. K. Kremer, Z. Anorg. Allg. Chem. **636**, 54 (2010).
[22]J. M. Law, C. Hoch, R. Glaum, I. Heinmaa, R. Stern, J. Kang, C. Lee, M.-H. Whangbo, and R. K. Kremer, Phys. Rev. B **83**, 180414(R) (2011).
[23]C. K. Majumdar and D. K. Ghosh, J. Math. Phys. **10**, 1388 (1969); **10**, 1399 (1969).
[24]M. Enderle, B. Fåk, H.-J. Mikeska, R. K. Kremer, A. Prokofiev, and W. Assmus, Phys. Rev. Lett. **104**, 237207 (2010).
[25]K. Brandt, Arkiv för Kemi, Mineralogi Och Geologi. A **17**, 1 (1943).
[26]N. Seferiadis and H. R. Oswald, Acta Crystallogr. Sect. C **43**, 10 (1986).
[27]M.-H. Whangbo, H.-J. Koo, and D. Dai, J. Solid State Chem. **176**, 417 (2003).
[28]D. Dai and M.-H. Whangbo, J. Chem. Phys. **114**, 2887 (2001); **118**, 29 (2003).
[29]G. Kresse and J. Hafner, Phys. Rev. B **47**, 558 (1993).
[30]G. Kresse and J. Furthmüller, Comput. Mater. Sci. **6**, 15 (1996).
[31]G. Kresse and J. Furthmüller, Phys. Rev. B **54**, 11169 (1996).
[32]J. P. Perdew, K. Burke, and M. Ernzerhof, Phys. Rev. Lett. **77**, 3865 (1996).
[33]S. L. Dudarev, G. A. Botton, S. Y. Savrasov, C. J. Humphreys, and A. P. Sutton, Phys. Rev. B **57**, 1505 (1998).
[34]H.-J. Koo and M.-H. Whangbo, Inorg. Chem. **47**, 128 (2008).
[35]H.-J. Koo and M.-H. Whangbo, Inorg. Chem. **47**, 4779 (2008).
[36]J. Kang, C. Lee, R. K. Kremer, and M.-H. Whangbo, J. Phys. Condens. Matter **21**, 392201 (2009).
[37]H.-J. Koo and M.-H. Whangbo, Inorg. Chem. **49**, 9253 (2010).
[38]J. Arsène, M. Lenglet, A. Erb, and P. Granger, Rev. Chim. Miner. **15**, 318 (1978).
[39]J. Rodriguez-Carvajal, Physica B **55**, 192 (1993).
[40]L. W. Johnson and S. P. McGlynn, Chem. Phys. Lett. **7**, 618 (1970).
[41]A. B. P. Lever, *Inorganic Electronic Spectroscopy* (Elsevier, Amsterdam, 1984).
[42]G. Kortüm, *Reflexionsspektroskopie* (Springer-Verlag, Berlin, 1969).
[43]B. N. Figgis and M. A. Hitchman, *Ligand Field Theory and Its Applications* (Wiley-VCH, New York, 2000).
[44]C. K. Jørgensen, R. Pappalardo, and H.-H. Schmidtke, J. Chem. Phys. **39**, 1422 (1963).
[45]D. E. Richardson, J. Chem. Ed. **70**, 372 (1993).
[46]E. Larsen and G. N. LaMar, J. Chem. Ed. **51**, 633 (1974).
[47]E. J. Baran, Spectrochim. Acta, Part A **50**, 2385 (1994).
[48]D. W. Smith, J. Chem. Phys. **50**, 2784 (1969).
[49]M. Bermejo and L. Pueyo, J. Chem. Phys. **78**, 854 (1983).
[50]H. G. Drickamer, *Electronic Transitions and the High Pressure Chemistry and Physics of Solids* (Chapman and Hall, London, 1973).
[51]M. Gerloch, *Magnetism and Ligand Field Theory* (Cambridge University Press, Cambridge, 1983).
[52]D. A. Cruse, J. E. Davies, J. H. Harding, M. Gerloch, D. J. Mackey, and R. F. McMeeking, *CAMMAG: A Fortran Program* (Cambridge University Press, Cambridge, 1980).
[53]D. S. McClure, in *Solid State Physics*, edited by F. Seitz and D. Turnbull, Vol. 9 (Academic, New York, 1959), p. 399.
[54]A. R. Miedema and L. J. deJongh, Adv. Phys. **23**, 1 (1974).
[55]D. H. Martin, *Magnetism in Solids* (MIT Press, Cambridge, MA, 1967).
[56]I. Yamada, M. Nishi, and J. Akimitsu, J. Phys. Condens. Matter **8**, 2625 (1996).
[57]H.-A. Krug von Nidda, L. E. Svistov, M. V. Eremin, R. M. Eremina, A. Loidl, V. Kataev, A. Validov, A. Prokofiev, and W. Assmus, Phys. Rev. B **65**, 134445 (2002).
[58]R. Kubo and K. Tomita, J. Phys. Soc. Jpn. **9**, 888 (1954).
[59]M. Oshikawa and I. Affleck, Phys. Rev. Lett. **82**, 5136 (1999).
[60]M. Oshikawa and I. Affleck, Phys. Rev. B **65**, 134410 (2002).
[61]P. W. Selwood, *Magnetochemistry*, 2nd ed. (Interscience, New York, 1956), p. 78.
[62]H. J. Xiang, C. Lee, and M.-H. Whangbo, Phys. Rev. B **76**, 220411(R) (2007).
[63]F. Heidrich-Meisner, A. Honecker, and T. Vekua, Phys. Rev. B **74**, 020403(R) (2006).
[64]For detailed numerical tables, see [http://www.theorie.physik.uni-goettingen.de/~honecker/j1j2-td/].
[65]R. L. Carlin, *Magnetochemistry* (Springer-Verlag, Berlin, 1986).
[66]D. C. Johnston, R. K. Kremer, M. Troyer, X. Wang, A. Klümper, S. L. Budko, A. F. Panchula, and P. C. Canfield, Phys. Rev. B **61**, 9558 (2000).
[67]C. Yasuda, S. Todo, K. Hukushima, F. Alet, M. Keller, M. Troyer, and H. Takayama, Phys. Rev. Lett. **94**, 217201 (2005). We note that the transverse interaction considered by Yasuda *et al.* is defined in terms of a single SE interaction to four nn within the plane perpendicular to the chain. As discussed below, the situation for $CuCrO_4$ is certainly more complex. We nevertheless use Yasuda's formulism to enable a comparison with other indirect observation of the interchain SE coupling.
[68]S. Seki, T. Kurumaji, S. Ishiwata, H. Matsui, H. Murakawa, Y. Tokunaga, Y. Kaneko, T. Hasegawa, and Y. Tokura, Phys. Rev. B **82**, 064424 (2010).
[69]R. K. Kremer (unpublished).